Energy Efficient Beamforming Schemes for Satellite-Aerial-Terrestrial Networks

Qingquan Huang, Min Lin, *Member, IEEE,* Jun-Bo Wang, *Member, IEEE,* Theodoros A. Tsiftsis, *Senior Member, IEEE,* and Jiangzhou Wang, *Fellow, IEEE*

Abstract

In this paper, we investigate energy efficient transmission for a satellite-aerial-terrestrial network (SATN), where a multi-antenna unmanned aerial vehicle (UAV) is employed as a relay to assist the satellite signal delivery. By considering total power constraint (TPC) or per-antenna power constraint (PPC) at the UAV, we first formulate an optimization problem to maximize the energy efficiency of the SATN, which is defined as ratio of the ergodic capacity to the total power consumption for communication at UAV. Then, by jointly exploiting array signal processing with the Dinkelbach's method, two new beamforming (BF) schemes, namely, TPC-BF and PPC-BF are proposed to solve the non-convex energy efficiency maximization problem. The main advantage of our method is that only angular information-based channel state information is used to obtain BF weight vectors so that a low implementation complexity is achieved. Furthermore, by assuming that the satellite-UAV link undergoes correlated Shadowed-Rician fading while the UAV-terminal link experiences correlated Rician fading, closed-form expressions for the statistics of the equivalent output signal-to-noise ratio are derived and, thus energy efficiency for the considered SATN with BF schemes is analytically presented. Finally, simulation results corroborate the derived expressions and confirm the effectiveness of the proposed BF schemes.

This work is supported by Key International Cooperation Research Project under Grant 61720106003. (*Corresponding author: Min Lin.)*

Q. Huang is with the Communications Engineering College, Army Engineering University of PLA, Nanjing 210007, China (e-mail: huangqingquan398@163.com).

M. Lin is with the College of Communication and Information Engineering, Nanjing University of Posts and Telecommunications, Nanjing 210016, China (e-mail: linmin@njupt.edu.cn).

J.-B. Wang is with the National Mobile Communications Research Laboratory, Southeast University, Nanjing 210096, China (email: jbwang@seu.edu.cn)

T. A. Tsiftsis is with the School of Intelligent Systems Science and Engineering, Jinan University (Zhuhai Campus), Zhuhai, 519070, China (e-mail: theodoros.tsiftsis@gmail.com)

J. Wang is with the School of Engineering and Digital Arts, University of Kent, Canterbury, Kent CT2 7NZ, United Kingdom (email: j.z.wang@kent.ac.uk).

Index Terms

Angular Information, Beamforming, Energy Efficiency, Satellite-Aerial-Terrestrial Network.

I. INTRODUCTION

With the on-going development of wireless communications, current terrestrial infrastructure can provide broadband services and ubiquitous access for million of users in high-density areas with low cost. However, there is still large population that lacks internet access in the rural or remote areas. Therefore, the integration of satellite components into the wireless system has received more and more attention due to its ability of offering high quality, great capacity and seamless coverage [1], [2]. For example, the fifth generation (5G) Infrastructure Public Private Partnership funded by European Commission and European Information and Communications Technology industry is looking at implementing satellite segment in future 5G systems [3].

A. Background and Motivation

In satellite communications (SatCom) system, the obstacles and shadowing between the satellite and the terrestrial terminal may make a line-of-sight (LoS) communication difficult to be maintained. To tackle this problem, the application of relay technology is considered as an effective and indispensable approach, resulting in a new architecture referred as integrated satellite and terrestrial relay network (ISTRN) which has been an active research topic in the open literature [4]. This architecture has also been adopted by the Digital Video-Broadcast Satellite services to Handhelds (DVB-SH) standard at frequencies below 3 GHz [5]. Furthermore, performance analysis results for ISTRN over Shadowed-Rician (SR) fading, while the terrestrial links are modeled as Nakagami-*m* with either amplify-and-forward (AF) [6]-[8] or decode-and-forward (DF) [9], [10] protocols have been published in the last years. Nevertheless, it is worth mentioning that the perfect channel state information (CSI) was assumed to be available in [6]-[10] so that the maximal-ratio combining (MRC) and maximal-ratio transmission (MRT) were utilized as the receive and transmit beamforming (BF) schemes, respectively.

Besides satellite and terrestrial cellular networks [11], [12], unmanned aerial vehicle (UAV) communication will play an important role in future wireless networks due to easy deployment, flexibility, and large coverage [13]-[16], especially in temporary large-scale events, disaster areas and marine communications. For example, Google and Facebook have demonstrated that aerial

platforms can be adopted to provide wireless internet access for various users. To exploit the spatial dimension and improve spectral efficiency (SE), UAVs typically adopt multi-antenna technology or massive antenna array to communicate with ground users [17], [18]. Under this circumstance, the BF technique that has the ability of spatial filter [19], [20], has been commonly applied in UAV communications. For example, a hierarchical beam search and codebook design method was proposed in [21] to enable fast BF training and tracking for UAV-based cellular networks. The authors of [22] proposed a linear precoding scheme based on the space alignment strategy and derived the optimal power allocation to maximize the achievable rate of the cognitive user subject to the power, interference, and relay's power constraints. Besides, by considering a dual-hop half-duplex DF relaying system with fixed wing UAVs, the joint design of beamforming and power allocation was proposed in [23] to obtain the maximal end-to-end signal-to-noise ratio (SNR) under transmit power constraints.

While the aforementioned works have significantly improved our understanding on how to maximize the throughput or the SE for an UAV system, the energy consumption is another important challenge in UAV-based communications. In fact, the battery-powered flying units have a very limited amount of energy that must be consumed by the communication platform and the UAV (or drone) hardware and mobility. Hence, it is important to efficiently manage the available energy so that the UAV operation time can be extended [24], [25]. The authors of [26] presented the power allocation framework to maximize the energy efficiency (EE) while satisfying the power budget, minimal rate, and interference constraints. In [27], the authors proposed a joint optimization design to obtain the maximal EE for a multi-antenna UAV relaying system with DF protocol over Rician fading channels. Recently, the satellite-aerial-terrestrial network (SATN) architecture [28] has been proposed as a promising candidate for emergency communications, which has been studied in the ABSOLUTE project [29]. In terms of EE maximization (EEM) in SATNs, an energy-efficient power allocation scheme was proposed in [30] for direct transmission with limited backhaul. Based on [30], the authors of [31] proposed a joint relay selection and power allocation scheme to realize EEM subject to power constraints, quality-of-service (QoS) requirements and backhaul capacity limitation. Nevertheless, the optimization design in [27], [30], [31] was based on the assumption of perfect CSI, which is rather overoptimistic in practical scenarios, mainly due to the estimation error and limited feedback burden, especially when UAV is deployed with a large number of antennas [32]-[34]. The latter observation motivates our current work presented in this paper.

B. Our Contribution

In this paper, we investigate the energy efficient transmission for a SATN, where a multi-antenna UAV is exploited as an aerial relay with AF protocol to aid the satellite communication. Unlike most of the existing related works, we utilize the angular information-based channel state information (AI-CSI) rather than the perfect CSI to conduct BF design. However, perfect CSI is difficult to be obtained especially in mobile scenarios. Since with the help of advanced array signal processing [35], angular information can be extracted more conveniently than the perfect CSI, our work is very valuable from an engineering perspective. Moreover, closed-form expressions for the EE of the considered network are derived.

In particular, our contributions can be summarized as follows:

- Compared with the existing related works, e.g. [6], [28], [30], [31], we develop a general analytical framework for energy efficient transmission of SATN, where the impact of antenna pattern, path loss, channel correlation and fading are considered. Specifically, we formulate a constrained optimization problem aiming at maximizing EE, while satisfying either total power constraint (TPC) or per-antenna power constraint (PPC), which are the two widely used power constraints in practice.
- By jointly using array signal processing (ASP) technology and the Dinkelbach's method, two new BF schemes are proposed to solve the non-convex EEM problem. One benefit of our method is that only AI-CSI is assumed to be available at UAV, which can significantly reduce the implementation complexity in comparison with the perfect CSI assumption considered in [6], [8], [22], [27], [30], [31]. The other benefit is that both the normalized BF weight vectors and the corresponding power coefficients are given in analytical expressions. Computer simulation results show that the performance gap between these two BF schemes and the optimal solution with perfect CSI is very small.
- By assuming that the satellite-UAV link undergoes correlated SR fading while the UAV-terminal link experiences correlated Rician fading, new theoretical formulas for the cumulative distribution function (CDF) of the equivalent output SNR are derived, based on which the exact analytical expressions for EE are further presented to quantify the performance of the considered SATN with various BF schemes.

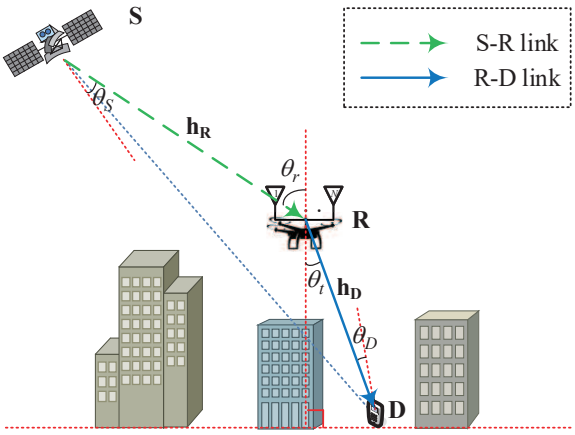

Fig. 1. System model of the considered network

C. Paper Organization and Notation

The rest of this paper is arranged as follows. In Section II, we describe the channel models and formulate the EEM problem. Then, by jointly use ASP technique with the Dinkelbach's method, two BF schemes are proposed in Section III. In Section IV, we derive accurate analytical expressions for the EE of the considered system with the two BF schemes. Section V provides simulation results along with discussions. Finally, conclusions are drawn in Section VI.

Notations: Bold uppercase and lowercase letters denote matrices and vectors, respectively, $(\cdot)^T$ and $(\cdot)^H$ indicate the transpose and Hermitian transpose operation, respectively, $\|\cdot\|$ and $|\cdot|$ denote Euclidean norm and absolute value, respectively, $\mathbb{E}[\cdot]$ represents the expectation, $diag(\cdot)$ the diagonal matrix, $\frac{\partial f(x)}{\partial x}$ the partial derivative operator, $\Pr\{A\}$ denotes the probability that event A occurs, $\mathbb{C}^{M\times N}$ denotes the complex space of $M\times N$, $\mathbb{N}(\mu,\sigma^2)$ and $\mathbb{CN}(\mu,\sigma^2)$ represent the real-valued and complex-valued Gaussian distribution with mean μ and covariance σ^2, respectively, $\mathbf{R}^{1/2}$ denotes the matrix square root of matrix $\mathbf{R}$, $\mathbf{I}_N$ denotes the N-dimensional unit matrix, $J_1(\cdot)$ and $J_3(\cdot)$ denote the first-kind Bessel function of order 1 and 3, respectively, $(a)_p = a(a+1)\cdots(a+p-1)$ is the Pochhammer symbol [36], ${}_1F_1(a,b,z)$ indicates the confluent hypergeometric function [36, eq. (9.210.1)], $\mathrm{G}_{p,q}^{m,n}[\cdot|\cdot]$ the Meijer-G function [36, eq. (9.301)].

II. System Model and Problem Formulation

As shown in Fig. 1, we consider a SATN, where the geostationary orbit (GEO) satellite (S) wants to send the messages to a ground terminal (D). However, due to the long distance and mask effect, the direct link between S and D is unavailable, hence a multirotor UAV hovered in

the air is utilized as a relay (R) to assist the satellite signal delivery. Moreover, it is assumed that S employs multibeam technology with single-feed-per-beam architecture [37] and R is equipped with an N-element uniform linear array (ULA), and D has a directional antenna. In what follows, we will introduce the channel models.

A. S-R Link Channel Model

To realistically model the S-R channel, the impact of satellite beam pattern, path loss, shadowing and small-scale fading should be taken into account. Mathematically, the channel vector of the S-R link can be expressed as [38]

$$\mathbf{h}_R = C_R \mathbf{g}_R, \tag{1}$$

with C_R being the coefficient given by

$$C_R = \lambda \sqrt{G_S G_R} \Big/ (4\pi d_R), \tag{2}$$

where λ denotes the wavelength, d_R is the distance between the satellite and UAV. Besides, G_S denotes the satellite beam pattern, which can be approximated as [38]

$$G_S \approx G_S^{\max} \left(\frac{J_1(u_S)}{2u_S} + 36 \frac{J_3(u_S)}{u_S^3} \right)^2, \tag{3}$$

where $G_S^{\max}$ is the maximum gain, and $u_S = 2.07123 \sin\theta_S / \sin\theta_{S,3dB}$, with θ_S being the off-axis angle with respect to the beam boresight, and $\theta_{S,3dB}$ is the 3dB beamwidth of satellite antenna. Without loss of generality, the element of antenna array at UAV can be considered omni-directional meaning that the receive antenna pattern $G_R = 1$ is satisfied.

In (1), $\mathbf{g}_R$ represents the shadowing and small-scale fading, which is usually modeled as composite fading distributions to describe the amplitude fluctuation of the signal envelope. Compared with some well-known mathematical models, such as Loo model and Corazza model, the SR model proposed in [39] is the more popular one, since it is more accurate with low computational burden. As a result, we here exploit SR to model the satellite link[1], which is a commonly used method in most of the related works, such as [4], [6], [28], [40]. Furthermore,

[1]Since the SR model accounts for the LoS scenarios with and without the effects of shadowing and fading, it is more general than the Nakagami-m or Rician channel models that has been adopted in UAV communications [28]. In this regard, SR is a commonly used channel model to describe the links between satellite and terrestrial terminal [4], [6], [40] as well as satellite and UAV [28].

in the scenarios where UAV acts as an aerial relay, the S-R link is composed of a predominant LoS propagation component and a sparse set of multi-path components with antenna correlation. In this regard, following a similar manner adopted in [41], the correlated channel model of the S-R link based on angular information can be expressed as

$$\mathbf{g}_R = \bar{\mathbf{g}}_R + \tilde{\mathbf{\Phi}}_R^{1/2} \tilde{\mathbf{g}}_R, \tag{4}$$

where the LoS component $\bar{\mathbf{g}}_R$ can be written as

$$\bar{\mathbf{g}}_R = Z_R \mathbf{a}(\theta_r), \tag{5}$$

with Z_R being a random variable (RV) obeying Nakagami-m distribution with average power Ω and severity parameter m, $\mathbf{a}(\theta_r)$ is the array steering vector given by

$$\mathbf{a}(\theta_r) = [1, exp(j\kappa d_e \sin\theta_r), \ldots, exp(j(N-1)\kappa d_e \sin\theta_r)]^T, \tag{6}$$

where $\kappa = 2\pi/\lambda$ is the wavenumber, θ_r denotes the angle-of-arrival (AoA) of incident signal, and d_e is the inter-element spacing of the array. In (4), $\tilde{\mathbf{\Phi}}_R^{1/2} \tilde{\mathbf{g}}_R$ represents the scattering component due to multi-path signals, with $\tilde{\mathbf{\Phi}}_R$ being the spatial correlation matrix (SCM) and $\tilde{\mathbf{g}}_R \in \mathbb{C}^{N\times 1}$ denotes the independent and identically distributed (i.i.d.) complex Gaussian RV satisfying $\tilde{\mathbf{g}}_R \sim \mathbb{CN}(\mathbf{0}, 2b\mathbf{I}_N)$, with $2b$ the average power of the scattering component.

B. R-D Link Channel Model

Based on [14], the channel vector $\mathbf{h}_D$ of the R-D link can be described by Rician fading combined with antenna pattern and path loss, which can be expressed as

$$\mathbf{h}_D = C_D \mathbf{g}_D, \tag{7}$$

where C_D in dB is given by [19]

$$C_D, dB = \frac{1}{2}(10\lg G_D + 20\lg\lambda - 10\alpha_D \lg d_D - 20\lg 4\pi), \tag{8}$$

where α_D denotes the path loss exponent corresponds to the environment, $d_D = \sqrt{H_R^2 + d_{RD}^2}$ with H_R being the height of UAV and d_{RD} the horizontal distance between UAV and the user. Besides,

the off-boresight antenna pattern G_D of the user is given by

$$G_D = \begin{cases} G_D^{\max} 10^{-\frac{3}{10}\left(\frac{2\theta_D}{\theta_{D,3dB}}\right)^2}, & |\theta_D| \le \frac{\theta_{D,ML}}{2} \\ G_D^{\mathrm{SLL}}, & \frac{\theta_{D,ML}}{2} \le |\theta_D| \le \frac{\pi}{2} \end{cases}, \tag{9}$$

where $G_D^{\max}$ and G_D^{SLL} denote the maximum gain and the averaged side-lobe gain, respectively, $\theta_{D,3dB}$ and $\theta_{D,ML}$ denote the 3dB beamwidth and main-lobe beamwidth, respectively.

Resorting to [14] and [42], the channel fading vector $\mathbf{g}_D \in \mathbb{C}^{N\times 1}$ in (7) is modeled as

$$\mathbf{g}_D = \sqrt{\frac{K}{K+1}}\bar{\mathbf{g}}_D + \sqrt{\frac{1}{K+1}}\tilde{\mathbf{\Phi}}_D^{1/2}\tilde{\mathbf{g}}_D, \tag{10}$$

where the Rician factor K denotes the ratio of the power of the specular component to the scattered components, $\bar{\mathbf{g}}_D = \mathbf{a}(\theta_t)$ represents the LoS component having a similar expression as (6) with θ_r replaced by the angle-of-departure (AoD) θ_t. In addition, $\tilde{\mathbf{\Phi}}_D^{1/2}\tilde{\mathbf{g}}_D$ represents the scattering components, with $\tilde{\mathbf{\Phi}}_D$ being the SCM and $\tilde{\mathbf{g}}_D$ satisfying $\tilde{\mathbf{g}}_D \sim \mathbb{CN}(\mathbf{0}, \mathbf{I}_N)$.

C. Problem Formulation

In this paper, we assume that the UAV relay works at half-duplex mode, hence the total communication between S and D occurs in two time slots. During the first time slot, S selects the best spot beam that covers the UAV, and sends the signal $x_S(t)$ with normalized power to R. After performing receive BF with normalized weight vector $\mathbf{w}_r \in \mathbb{C}^{N\times 1}$, the output signal at R can be expressed as

$$y_R(t) = \mathbf{w}_r^H\left(\sqrt{P_S}\mathbf{h}_R x_S(t) + \mathbf{n}_R(t)\right), \tag{11}$$

where P_S denotes the satellite transmit power. During the second time slot, owing to the fact that perfect CSI is unavailable at R, UAV first amplifies the received signal $y_R(t)$ with fixed gain G as

$$G = \sqrt{P_R \Big/ \left(\mathbb{E}\left[P_S\left|\mathbf{w}_r^H\mathbf{h}_R\right|^2\right] + \sigma_R^2\right)}, \tag{12}$$

where P_R denotes the transmit power of UAV. Then the amplified signal is forwarded to D after performing transmit BF with normalized weight vector $\mathbf{w}_t \in \mathbb{C}^{N\times 1}$. Consequently, the received signal at D can be written as

$$\begin{aligned} y_D(t) &= \mathbf{h}_D^H\mathbf{w}_t G y_R(t) + n_D(t) \\ &= G\sqrt{P_S}\mathbf{h}_D^H\mathbf{w}_t\mathbf{w}_r^H\mathbf{h}_R x_S(t) + G\mathbf{h}_D^H\mathbf{w}_t\mathbf{w}_r^H\mathbf{n}_R(t) + n_D(t). \end{aligned} \tag{13}$$

Without loss of generality, we suppose that the additive white Gaussian noise (AWGN) at R and D satisfy $\mathbf{n}_R(t) \sim \mathbb{CN}\left(\mathbf{0}, \sigma_R^2 \mathbf{I}_N\right)$ and $n_D(t) \sim \mathbb{CN}\left(0, \sigma_D^2\right)$, respectively.

By substituting (1), (7) and (12) into (13), the instantaneous output SNR at D can be expressed as

$$\gamma = \frac{G^2 P_S \left|\mathbf{w}_r^H \mathbf{h}_R\right|^2 \left|\mathbf{h}_D^H \mathbf{w}_t\right|^2}{G^2 \left|\mathbf{h}_D^H \mathbf{w}_t\right|^2 \left|\mathbf{w}_r^H \mathbf{n}_R\right|^2 + \sigma_D^2} = \frac{\frac{P_S C_R^2}{\sigma_R^2}\left|\mathbf{w}_r^H \mathbf{g}_R\right|^2 \frac{P_R C_D^2}{\sigma_D^2}\left|\mathbf{g}_D^H \mathbf{w}_t\right|^2}{\frac{P_R C_D^2}{\sigma_D^2}\left|\mathbf{g}_D^H \mathbf{w}_t\right|^2 + \frac{P_R}{G^2 \sigma_R^2}} \triangleq \frac{\gamma_1 \gamma_2}{\gamma_2 + C}, \tag{14}$$

where

$$\gamma_1 = \frac{P_S C_R^2}{\sigma_R^2}\left|\mathbf{w}_r^H \mathbf{g}_R\right|^2 \triangleq \frac{P_S}{\rho_R^2}\left|\mathbf{w}_r^H \mathbf{g}_R\right|^2, \tag{15}$$

$$\gamma_2 = \frac{P_R C_D^2}{\sigma_R^2}\left|\mathbf{g}_D^H \mathbf{w}_t\right|^2 \triangleq \frac{P_R}{\rho_D^2}\left|\mathbf{w}_t^H \mathbf{g}_D\right|^2, \tag{16}$$

and

$$C = \mathbb{E}\left[\gamma_1\right] + 1. \tag{17}$$

In addition, according to [4], the total power consumption for communications at UAV is given by

$$P_{tot} = \mu P_R + P_{const} \tag{18}$$

where $\mu \geq 1$ denotes the power amplifier inefficiency coefficient, $P_{const} = NP_c + P_0$ with P_c being the circuit power consumption of each antenna and P_0 denoting the static power at UAV independent of the number of antennas. To balance the system throughput and the total power consumption at the UAV, EE in unit bit/J is often used as the performance metric, which is defined as [4], [43]

$$\eta = \frac{B\mathbb{E}\left[\log_2(1+\gamma)\right]/2}{\mu P_R + P_{const}} \triangleq \frac{R_{EC}}{P_{tot}}, \tag{19}$$

where R_{EC} denotes the ergodic capacity (EC) of the system, with B denoting the bandwidth and the factor $1/2$ is owing to the fact that the communication occurs at two time slots.

In this paper, we propose two BF schemes to obtain the EEM for the considered SATN under different power constraints. Furthermore, the EE of the considered system with each BF scheme is also analyzed through the derivation of new analytical expressions.

III. Proposed BF Schemes

In this section, we first formulate a constrained optimization problem to realize EEM subject to either TPC or PPC at UAV. Then, based on the AI-CSI, we exploit the array signal processing technologies and Dinkelbach's approach, and two BF schemes are finally proposed.

A. TPC-BF Scheme

In this subsection, we consider the scenario of TPC at UAV. In this regard, the constrained optimization problem for EEM can be formulated as

$$\max_{P_R,\mathbf{w}_r,\mathbf{w}_t} \quad \eta = \frac{B\mathbb{E}\left[\ln\left(1+\gamma\right)\right]}{\left(\mu P_R + P_{const}\right)2\ln 2} \tag{20a}$$

$$\text{s.t.} \quad \|\mathbf{w}_r\| = 1, \|\mathbf{w}_t\| = 1, P_R \le P_{R,\max}. \tag{20b}$$

where the TPC results in the constraint of (20b), with $P_{R,\max}$ being the maximal transmit power constraint at the UAV. Since the S-R and R-D links follow correlated SR and correlated Rician distribution, respectively, the analytical expression of R_{EC} is so complex that makes (20) mathematically intractable. In this regard, similar to most of the related works, such as [44], [45], we use the Jensen's inequality and obtain an upper bound of R_{EC} as

$$R_{EC} \le \frac{B}{2\ln 2}\ln\left(1+\mathbb{E}\left[\gamma\right]\right) \tag{21}$$

where

$$\begin{aligned}\mathbb{E}\left[\gamma\right] &\overset{a}{=} \mathbb{E}_{\mathbf{g}_R,\mathbf{g}_D}\left[\frac{\left(\mathbf{w}_r^H\mathbf{g}_R\mathbf{g}_R^H\mathbf{w}_r P_S/\rho_R^2\right)P_R\left(\mathbf{w}_t^H\mathbf{g}_D\mathbf{g}_D^H\mathbf{w}_t/\rho_D^2\right)}{P_R\left(\mathbf{w}_t^H\mathbf{g}_D\mathbf{g}_D^H\mathbf{w}_t/\rho_D^2\right)+\mathbb{E}\left[\mathbf{w}_r^H\mathbf{g}_R\mathbf{g}_R^H\mathbf{w}_r P_S/\rho_R^2\right]+1}\right] \\ &\overset{b}{\approx} \frac{P_R\mathbf{w}_r^H\mathbf{\Phi}_R\mathbf{w}_r\mathbf{w}_t^H\mathbf{\Phi}_D\mathbf{w}_t P_S/\left(\rho_R^2\rho_D^2\right)}{P_R\mathbf{w}_t^H\mathbf{\Phi}_D\mathbf{w}_t/\rho_D^2+\mathbf{w}_r^H\mathbf{\Phi}_R\mathbf{w}_r P_S/\rho_R^2+1}\end{aligned} \tag{22}$$

In the step b, we have taken the first term of the Taylor's series for the expectation. It is worth mentioning that the tightness of this approximation (21)-(22) will be confirmed through the simulation results in Section V, and similar analytical proof can be found in [45]. In (22), $\mathbf{\Phi}_R = \mathbb{E}_{\mathbf{g}_R}\left[\mathbf{g}_R\mathbf{g}_R^H\right]$ and $\mathbf{\Phi}_D = \mathbb{E}_{\mathbf{g}_D}\left[\mathbf{g}_D\mathbf{g}_D^H\right]$ are the channel correlation matrices (CCMs) of $\mathbf{g}_R$ and $\mathbf{g}_D$, respectively. In most of related works, CCM is always obtained through accumulation of the CSI. However, in this paper, we propose to obtain the CCMs by using statistical angular information, which is presented in Lemma 1.

Lemma 1. *The mn-th element of the CCMs $\mathbf{\Phi}_R$ and $\mathbf{\Phi}_D$ can be, respectively, approximated as*

$$[\mathbf{\Phi}_R]_{m,n} \approx e^{j(m-n)\kappa d_e \sin\theta_r} \times \begin{cases} (\Omega + 2b\frac{\sin((m-n)u_1)}{(m-n)u_1}), & \text{case I} \\ (\Omega + 2b\mathrm{e}^{-(m-n)^2 u_2}), & \text{case II} \end{cases} \tag{23}$$

$$[\mathbf{\Phi}_D]_{m,n} \approx e^{j(m-n)\kappa d_e \sin\theta_t} \times \begin{cases} (\frac{K}{K+1} + \frac{1}{K+1}\frac{\sin((m-n)v_1)}{(m-n)v_1}), & \text{case I} \\ (\frac{K}{K+1} + \frac{1}{K+1}\mathrm{e}^{-(m-n)^2 v_2}), & \text{case II} \end{cases} \tag{24}$$

where $u_1 = \kappa d_e \frac{\Delta_r}{2}\cos\theta_r$, $u_2 = \frac{\Delta_r^2}{32}(\kappa d_e \cos\theta_r)^2$, $v_1 = \kappa d_e \frac{\Delta_t}{2}\cos\theta_t$, $v_2 = \frac{\Delta_t^2}{32}(\kappa d_e \cos\theta_t)^2$ with Δ_r and Δ_t being the angular spread associated with AoA θ_r and AoD θ_t, respectively. Besides, case I and case II denote, respectively, the scenarios that the powers of scattering components in (4) and (10) obey uniform distribution and Gaussian distribution.

Proof. See Appendix A. □

Based on Lemma1, we can first calculate the CCMs simply by using the signal AoA/AoD and angular spread, which are much easier to be obtained than the CSI. Next, with the help of the derived CCMs, we can design the TPC-BF scheme to solve the EEM problem in (20). Using (21)-(24) into (20), the EEM problem can be reformulated as

$$\max_{P_R, \mathbf{w}_r, \mathbf{w}_t} \quad \frac{B\ln\left(1 + \frac{P_R \mathbf{w}_r^H \mathbf{\Phi}_R \mathbf{w}_r \mathbf{w}_t^H \mathbf{\Phi}_D \mathbf{w}_t P_S / (\rho_R^2 \rho_D^2)}{P_R \mathbf{w}_t^H \mathbf{\Phi}_D \mathbf{w}_t / \rho_D^2 + \mathbf{w}_r^H \mathbf{\Phi}_R \mathbf{w}_r P_S / \rho_R^2 + 1}\right)}{(\mu P_R + P_{const}) 2\ln 2} \tag{25a}$$

$$\text{s.t.} \quad \|\mathbf{w}_r\| = 1, \|\mathbf{w}_t\| = 1, P_R \le P_{R,\max}. \tag{25b}$$

In fact, if the transmit power P_R is fixed, the objective function in (25a) monotonically increases with $\mathbf{w}_r^H \mathbf{\Phi}_R \mathbf{w}_r$ and $\mathbf{w}_t^H \mathbf{\Phi}_D \mathbf{w}_t$. With this regard, we can first exploit ASP technologies to calculate the normalized BF weight vectors $\mathbf{w}_r$ and $\mathbf{w}_t$, and then conduct the optimal power allocation with Dinkelbach's approach to realize the EEM. To this end, the following two optimization problems can be established to obtain the normalized BF weight vectors, namely,

$$\max_{\mathbf{w}_r} \ \mathbf{w}_r^H \mathbf{\Phi}_R \mathbf{w}_r, \ \text{s.t.} \ \|\mathbf{w}_r\| = 1, \tag{26}$$

$$\max_{\mathbf{w}_t} \ \mathbf{w}_t^H \mathbf{\Phi}_D \mathbf{w}_t, \ \text{s.t.} \ \|\mathbf{w}_t\| = 1. \tag{27}$$

Using the spectral theorem results in

$$\mathbf{\Phi}_R = [\mathbf{u}_{R1}, \mathbf{u}_{R2}, \ldots, \mathbf{u}_{RN}]\, diag\,(\lambda_{R1}, \lambda_{R2}, \ldots, \lambda_{RN})\, [\mathbf{u}_{R1}, \mathbf{u}_{R2}, \ldots, \mathbf{u}_{RN}]^H, \tag{28}$$

where $\lambda_{R\mathrm{n}}$'s are the eigenvalues arranged in a nonincreasing order, and $\mathbf{u}_{Rn}$'s are the corresponding eigenvectors. By substituting (28) into (26), it is not difficult to find that

$$\mathbf{w}_r^H \mathbf{\Phi}_R \mathbf{w}_r \leq \lambda_{R1}. \tag{29}$$

The equality holds only when

$$\mathbf{w}_{r,TPC}^* = \mathbf{u}_{R1}. \tag{30}$$

With a similar manner, since $\mathbf{\Phi}_D$ can be decomposed as

$$\mathbf{\Phi}_D = [\mathbf{u}_{D1}, \mathbf{u}_{D2}, \ldots, \mathbf{u}_{DN}]\, diag\left(\lambda_{D1}, \lambda_{D2}, \ldots, \lambda_{DN}\right) [\mathbf{u}_{D1}, \mathbf{u}_{D2}, \ldots, \mathbf{u}_{DN}]^H, \tag{31}$$

the optimal BF weight vector for (27) can be written as

$$\mathbf{w}_{t,TPC}^* = \mathbf{u}_{D1}. \tag{32}$$

Next, we focus on the power allocation. By substituting (28)-(32) into (25), the original constrained EEM problem can be simplified as

$$\max_{P_R} \ \eta = \frac{B \ln\left(1 + P_R\left(\beta - 1\right)\alpha / \left(P_R \alpha + \beta\right)\right)}{\left(\mu P_R + P_{const}\right) 2 \ln 2} \tag{33a}$$

$$\text{s.t. } P_R \leq P_{R,\max}. \tag{33b}$$

where $\alpha = \lambda_{D1}/\rho_D^2$, $\beta = 1 + \lambda_{R1} P_S / \rho_R^2$. Owing to the fractional form, the objective function of (33a) is non-convex and hard to solve. To tackle this difficulty, by resorting to the Dinkelbach's approach [46], [47], we consider the following problem with subtractive form as

$$g\left(\eta\right) = \arg\max_{P_R} \ B \ln\left(1 + P_R\left(\beta - 1\right)\alpha / \left(P_R \alpha + \beta\right)\right) - \eta\left(\mu P_R + P_{const}\right) 2 \ln 2 \tag{34a}$$

$$\text{s.t.} \quad P_R \leq P_{R,\max}. \tag{34b}$$

If η^* denotes the maximum EE, the problems (33) and (34) are equivalent if and only if $g\left(\eta^*\right) = 0$ holds, a similar proof can be found in Appendix A in [48]. Therefore, in the sequel, we exploit the iterative method to obtain the value of η satisfying $g\left(\eta\right) = 0$. For the i-th iteration, η in (34a) is replaced with η^i. By differentiating (34a) with respect to P_R and setting the result to zero, the

saddle point at i-th iteration is given by

$$P_R^i = \begin{cases} \sqrt{\left(\frac{\beta+1}{2\alpha}\right)^2 + \frac{B(\beta-1)}{2\eta^i \mu\alpha \ln 2} - \frac{\beta}{\alpha^2}} - \frac{\beta+1}{2\alpha}, & \eta^i > \eta_{th} \\ P_{R,\max}, & \eta^i \le \eta_{th} \end{cases} \tag{35}$$

where $\eta_{th} = \frac{(\beta-1)\alpha}{2\mu\left(\alpha^2\left(P_R^{\max}\right)^2+(\beta+1)\alpha P_R^{\max}+\beta\right)\ln 2}$. In (35), $P_R^i = P_R^{\max}$ for the case of $\eta^i \le \eta_{th}$ is due to the maximum transmit power constraint. Therefore, we obtain P_R^i at the i-th iteration for given η^i by using (35). Furthermore, it is used to update $\eta^{i+1} = \frac{B\ln\left(1+P_R^i(\beta-1)\alpha\left/\left(P_R^i\alpha+\beta\right)\right.\right)}{\left(\mu P_R^i+P_{const}\right)2\ln 2}$ for the next iteration until the terminal condition $\left|\eta^{i+1}-\eta^i\right| \le \varepsilon$ is satisfied, where ε is the pre-determined tolerance.

Since $\ln(1+x) \le x$, by applying it to η in (33a), the second term of the first case for P_R^i in (35) satisfies

$$\begin{aligned} \frac{B(\beta-1)}{2\eta^i\mu\alpha\ln 2} - \frac{\beta}{\alpha^2} &\ge \frac{\left(\mu P_R^{i-1}+P_{const}\right)2\ln 2}{P_R^{i-1}(\beta-1)\alpha\left/\left(P_R^{i-1}\alpha+\beta\right)\right.} \frac{\beta+1}{2\mu\alpha\ln 2} - \frac{\beta}{\alpha^2} \\ &= \frac{\beta}{\alpha^2}\left(\left(1+P_{const}\left/\left(\mu P_R^{i-1}\right)\right.\right)\left(1+P_R^{i-1}\alpha\left/\beta\right.\right)-1\right) \ge 0. \end{aligned} \tag{36}$$

By substituting (36) into (35), one obtain that $P_R^i \ge 0$, hence P_R^i calculated by (35) in i-th iteration is always non-negative.

Finally, the power allocation scheme for EEM problem in (33) can be summarized as Algorithm 1, shown at the top of next page. The proposed Algorithm 1 converges to the optimal solution of problem (34), and a similar proof can be found in [47].

Algorithm 1: Optimal power allocation scheme

1 Initialize $i = 0$ and set $\eta^0 = \frac{B\ln\left(1+P_R^{\max}(\beta-1)\alpha\left/\left(P_R^{\max}\alpha+\beta\right)\right.\right)}{\left(\mu P_R^{\max}+P_{const}\right)2\ln 2}$;
2 **repeat**
3 Compute P_R^i through (35) and then update $\eta^{i+1} = \frac{B\ln\left(1+P_R^i(\beta-1)\alpha\left/\left(P_R^i\alpha+\beta\right)\right.\right)}{\left(\mu P_R^i+P_{const}\right)2\ln 2}$;
4 Calculate $\vartheta = \left|\eta^{i+1}-\eta^i\right|$;
5 Set $i = i+1$.
6 **until** $\vartheta \le \varepsilon$, *with* ε *being the pre-determined tolerance*;
7 Obtain the optimal transmit power with $P_R^* = P_R^i$.

B. PPC-BF Scheme

In some scenarios, each transmit antenna is equipped with its own power amplifier in its analog front-end. Thus, this subsection focuses on the PPC of the UAV, which is more realistic

than the commonly used TPC [49].

First of all, following (19), (21) and (22), the constrained EEM problem can be formulated as

$$\max_{P_R,\mathbf{w}_r,\mathbf{w}_t} \quad \frac{B\ln\left(1+\frac{P_R\mathbf{w}_r^H\mathbf{\Phi}_R\mathbf{w}_r\mathbf{w}_t^H\mathbf{\Phi}_D\mathbf{w}_tP_S/\left(\rho_R^2\rho_D^2\right)}{P_R\mathbf{w}_t^H\mathbf{\Phi}_D\mathbf{w}_t/\rho_D^2+\mathbf{w}_r^H\mathbf{\Phi}_R\mathbf{w}_rP_S/\rho_R^2+1}\right)}{\left(\mu P_R+P_{const}\right)2\ln 2} \tag{37a}$$

$$\text{s.t.} \quad |[\mathbf{w}_r]_i|^2=1/N, |[\mathbf{w}_t]_i|^2=1/N, P_R\le P_R^{\max}, \tag{37b}$$

where the constraint (37b) is owing to the PPC at UAV, with $[\mathbf{w}_r]_i$ and $[\mathbf{w}_t]_i$ denoting the i-th elements of $\mathbf{w}_r$ and $\mathbf{w}_t$, respectively, and $P_{R,\max}$ the maximal transmit power constraint at the UAV. With a similar approach followed in Section III-A, we obtain the normalized BF weight vectors via ASP technologies and optimal power coefficient through Dinkelbach's approach separately. As for the former purpose, the following two optimization problems can be formulated, namely,

$$\max_{\mathbf{w}_r} \quad \mathbf{w}_r^H\mathbf{\Phi}_R\mathbf{w}_r, \text{ s.t. } |[\mathbf{w}_r]_i|^2=1/N, \tag{38}$$

$$\max_{\mathbf{w}_t} \quad \mathbf{w}_r^H\mathbf{\Phi}_D\mathbf{w}_t, \text{ s.t. } |[\mathbf{w}_t]_i|^2=1/N. \tag{39}$$

For case I that the scattering power obeys the uniform distribution, by using the Taylor's expansion as $\mathbf{a}\left(\theta_r+\tilde{\theta}_r\right)\approx\mathbf{a}\left(\theta_r\right)+\tilde{\theta}_r\mathbf{d}_1+\tilde{\theta}_r^2\mathbf{d}_2/2$ with $\mathbf{d}_1=\partial\mathbf{a}(\theta_r)/\partial\theta_r$ and $\mathbf{d}_2=\partial^2\mathbf{a}(\theta_r)/\partial\theta_r^2$ in (71) of Appendix A, $\tilde{\mathbf{\Phi}}_R$ can be approximated as

$$\begin{aligned}
\tilde{\mathbf{\Phi}}_R &\approx \int_{-\Delta_r/2}^{\Delta_r/2} f_{\tilde{\theta}_r}\left(\tilde{\theta}_r\right)\left(\mathbf{a}\left(\theta_r\right)+\tilde{\theta}_r\mathbf{d}_1+\tilde{\theta}_r^2\mathbf{d}_2/2\right)(\cdots)^H d\tilde{\theta}_r \\
&= \int_{-\Delta_r/2}^{\Delta_r/2} f_{\tilde{\theta}_r}\left(\tilde{\theta}_r\right)\left(\mathbf{a}\left(\theta_r\right)\mathbf{a}^H\left(\theta_r\right)+\tilde{\theta}_r\left(\mathbf{a}\left(\theta_r\right)\mathbf{d}_1^H+\mathbf{d}_1\mathbf{a}^H\left(\theta_r\right)\right)\right. \\
&\left.+\tilde{\theta}_r^2\left(\mathbf{d}_1\mathbf{d}_1^H+\mathbf{d}_2\mathbf{a}^H\left(\theta_r\right)/2+\mathbf{a}\left(\theta_r\right)\mathbf{d}_2^H/2\right)+\tilde{\theta}_r^3\left(\mathbf{d}_1\mathbf{d}_2^H/2+\mathbf{d}_1^H\mathbf{d}_2/2\right)+\tilde{\theta}_r^4\mathbf{d}_2\mathbf{d}_2^H/4\right)d\tilde{\theta}_r \\
&\approx \mathbf{a}\left(\theta_r\right)\mathbf{a}^H\left(\theta_r\right)+\frac{\Delta_r^2}{12}\left(\mathbf{d}_2\mathbf{a}^H\left(\theta_r\right)+\mathbf{a}\left(\theta_r\right)\mathbf{d}_2^H+2\mathbf{d}_1\mathbf{d}_1^H\right) \\
&\approx \frac{1}{2}\left(\left(\mathbf{a}\left(\theta_r\right)+\mathbf{d}_1\Delta_r\Big/\sqrt{6}+\mathbf{d}_2\Delta_r^2\Big/\sqrt{12}\right)(\cdots)^H+\left(\mathbf{a}\left(\theta_r\right)-\mathbf{d}_1\Delta_r\Big/\sqrt{6}+\mathbf{d}_2\Delta_r^2\Big/\sqrt{12}\right)(\cdots)^H\right) \\
&\approx \frac{1}{2}\left(\mathbf{a}\left(\theta_r+\Delta_r\Big/\sqrt{6}\right)(\cdots)^H+\mathbf{a}\left(\theta_r-\Delta_r\Big/\sqrt{6}\right)(\cdots)^H\right)
\end{aligned} \tag{40}$$

With a similar manner, $\tilde{\mathbf{\Phi}}_R$ for case II that the scattering power follows the Gaussian distribution,

can be approximated as

$$\tilde{\mathbf{\Phi}}_R \approx \frac{1}{2}\left(\mathbf{a}\left(\theta_r + \frac{\Delta_r}{\sqrt{8}}\right)(\cdots)^H + \mathbf{a}\left(\theta_r - \frac{\Delta_r}{\sqrt{8}}\right)(\cdots)^H\right) \tag{41}$$

Since the S-R link is highly correlated due to the lack of scattering, Δ_r is always small enough so that $\tilde{\mathbf{\Phi}}_R \approx \mathbf{a}(\theta_r)\mathbf{a}^H(\theta_r)$ is satisfied for both case I and II. By using (40) and (41) into (70), the CCM $\mathbf{\Phi}_R$ can be approximated as

$$\mathbf{\Phi}_R \approx (\Omega + 2b)\,\mathbf{a}(\theta_r)\,\mathbf{a}^H(\theta_r) \tag{42}$$

Thus, the normalized receive BF weight vector $\mathbf{w}_r$ for (38) is given by

$$\mathbf{w}_{r,PPC}^* = \mathbf{a}(\theta_r) \Big/ \sqrt{N}. \tag{43}$$

With a similar manner, $\mathbf{\Phi}_D$ can also be approximated as

$$\mathbf{\Phi}_D \approx \mathbf{a}(\theta_t)\,\mathbf{a}^H(\theta_t), \tag{44}$$

and the normalized transmit BF weight vector $\mathbf{w}_t$ for (39) can be obtained as

$$\mathbf{w}_{t,PPC}^* = \mathbf{a}(\theta_t) \Big/ \sqrt{N}. \tag{45}$$

Furthermore, by denoting $\alpha = \mathbf{a}^H(\theta_t)\mathbf{\Phi}_D\mathbf{a}(\theta_t)/\left(N\rho_D^2\right)$ and $\beta = 1 + \mathbf{a}^H(\theta_r)\mathbf{\Phi}_R\mathbf{a}(\theta_r)P_S/\left(N\rho_R^2\right)$, the power allocation method for the PPC-BF scheme is similar to Algorithm 1.

Until now, the TPC-BF and PPC-BF schemes have been proposed. As opposed to the perfect CSI assumption in most of the existing works [6], [8], [22], [30], [31], we focus on the scenarios of UAV application by exploiting the angular information-based CSI. Moreover, we propose two new BF schemes and analytical expressions are derived. Compared with TPC-BF scheme, which needs to perform singular value decomposition on the CCMs, the PPC-BF scheme directly use the signal AOA and AOD to conduct beamforming design, thus has the benefit of lower complexity. Besides, since only the phase of each array element is needed to be controlled in PPC-BF scheme, it can be implemented with analog processing, which avoids the high energy consumption and computational burden of digital processing units. Moreover, the numerical results in Section V show that the PPC-BF scheme can achieve as nearly equivalent EE to that of TPC-BF scheme.

IV. Energy Efficiency Analysis

This section aims at deriving a uniform analytical EE expression for the considered SATN with the proposed two BF schemes. For notational brevity, we denote $\mathbf{w}_r$, $\mathbf{w}_t$ and P_R as the optimal receive BF weight vector, transmit BF weight vector and power coefficient, respectively, regardless of what kind of scheme is employed.

Although Jensen's inequality is a widely used approach to evaluate the ergodic capacity, R_{EC}, sometimes its accuracy can't be satisfied at low SNR. In this regard, we write the exact expression of R_{EC} in (19) as

$$\begin{aligned} R_{EC} &= \frac{B}{2\ln 2}\mathbb{E}\left[\ln\left(1+\frac{\gamma_1\gamma_2}{\gamma_2+C}\right)\right] \\ &= \frac{B}{2\ln 2}\left(\mathbb{E}\left[\ln\left(1+\frac{\gamma_2}{C}\left(\gamma_1+1\right)\right)\right]-\mathbb{E}\left[\ln\left(1+\frac{\gamma_2}{C}\right)\right]\right) \\ &= \frac{B}{2\ln 2}\mathbb{E}\left[\ln\left(1+\gamma^{'}\right)\right]-\frac{B}{2\ln 2}\mathbb{E}\left[\ln\left(1+Z\right)\right] \\ &\triangleq R_{\gamma^{'}}-R_Z, \end{aligned} \tag{46}$$

where $\gamma^{'}=Z\gamma_1$, $Z=\frac{\gamma_2}{C}$ and $\gamma_1^{'}=\gamma_1+1$. Since Z and $\gamma_1^{'}$ are RVs composite of Rician and Shadowed Rician RVs, respectively, the probability density function (PDF) of $\gamma^{'}$ is complex, leading to that the evaluation of $R_{\gamma^{'}}$ is not very straightforward. Hence, we first condition on $Z=z$ to compute the conditional expression for $R_{\gamma^{'}|Z}$ and then seek for the expectation of Z. Therefore, $R_{\gamma^{'}}$ can be calculated as

$$R_{\gamma^{'}}=\int_0^{\infty}R_{\gamma^{'}|Z}f_Z\left(z\right)dz. \tag{47}$$

Here, by using the moment generating function (MGF) approach, $R_{\gamma^{'}|Z}$ can be expressed as [40]

$$R_{\gamma^{'}|Z}=\frac{B}{2\ln 2}\mathbb{E}\left[\ln\left(1+\gamma^{'}|z\right)\right]=\frac{B}{2\ln 2}\int_0^{\infty}\frac{e^{-s}}{s}\left(1-\mathcal{M}_{\gamma^{'}}\left(s|z\right)\right)ds, \tag{48}$$

where the conditional MGF of $\gamma^{'}$ can be determined as

$$\mathcal{M}_{\gamma^{'}}\left(s|z\right)=\mathcal{M}_{\gamma_1^{'}}\left(zs|z\right)=1-zs\int_0^{\infty}e^{-zsx}\left(1-F_{\gamma_1^{'}}\left(x\right)\right)dx. \tag{49}$$

By using (48) and (49) into (47), $R_{\gamma^{'}}$ can be denoted by

$$R_{\gamma^{'}} = \frac{B}{2\ln 2}\int_0^\infty z f_Z(z) \underbrace{\int_0^\infty e^{-s}\underbrace{\left(\int_0^\infty e^{-zsx}\left(1-F_{\gamma_1^{'}}(x)\right)dx\right)}_{I_1} ds}_{I_2} dz. \tag{50}$$

In order to calculate the integrations I_1 and I_2 in (50), we should first derive the CDF of $\gamma_1^{'} = \gamma_1 + 1$ and PDF of $Z = \frac{\gamma_2}{C}$. To this end, the analytical CDF expression of γ_1 and PDF expression of γ_2 are first presented in Lemma 2.

Lemma 2. *The CDF of γ_1 and PDF of γ_2 are, respectively, given by*

$$F_{\gamma_1}(x) = 1 - a_1 \sum_{k=0}^{m-1} \frac{(1-m)_k (-a_2)^k}{l^{k+1}(1)_k} e^{-\frac{lx}{\bar{\gamma}_1}} \sum_{n=0}^{k} \frac{l^n}{\bar{\gamma}_1^n n!} x^n, \tag{51}$$

$$f_{\gamma_2}(x) = \frac{e^{-Z_D^2/(2b_D)}}{2b_D\bar{\gamma}_2} e^{-\frac{x}{2b_D\bar{\gamma}_2}} I_0\left(\frac{Z_D}{b_D}\sqrt{\frac{x}{\bar{\gamma}_2}}\right), \tag{52}$$

where $q = (1+p-v)/2$, $l = 1/(2b_R) - a_2$, $b_R = b\left\|\mathbf{w}_r^H \tilde{\mathbf{\Phi}}_R^{1/2}\right\|^2$, $Z_D = \sqrt{K/(K+1)}\left|\mathbf{w}_t^H \mathbf{a}(\theta_t)\right|$, $b_D = \left\|\mathbf{w}_t^H \tilde{\mathbf{\Phi}}_D^{1/2}\right\|^2/(2(K+1))$, a_1, a_2 *and* C *can be, respectively, expressed as*

$$a_1 = \frac{1}{2b_R}\left(\frac{2b_R m}{2b_R m + \left|\mathbf{w}_r^H \mathbf{a}(\theta_r)\right|^2 \Omega}\right)^m, \tag{53}$$

$$a_2 = \frac{\left|\mathbf{w}_r^H \mathbf{a}(\theta_r)\right|^2 \Omega}{2b_R\left(2b_R m + \left|\mathbf{w}_r^H \mathbf{a}(\theta_r)\right|^2 \Omega\right)}, \tag{54}$$

$$C = 1 + \bar{\gamma}_1 a_1 \sum_{k=0}^{m-1} \frac{(1-m)_k (-a_2)^k (k+1)}{(1)_k (1/(2b_R) - a_2)^{k+2}}. \tag{55}$$

Proof. See Appendix B. □

It should be noted that we here take a reasonable assumption of $m \in N^+$ for analytical tractability [4, 50]. Then with the help of (51) and $F_{\gamma_1^{'}}(x) = F_{\gamma_1}(x-1)$, I_1 can be calculated as

$$I_1 = a_1 e^{\frac{l}{\bar{\gamma}_1}} \sum_{k=0}^{m-1} \frac{(1-m)_k (-a_2)^k}{l^{k+1}(1)_k} \sum_{n=0}^{k} \frac{l^n}{\bar{\gamma}_1^n n!} \sum_{v=0}^{n} \binom{n}{v} (-1)^{n-v} \int_0^\infty e^{-\left(zs+\frac{l}{\bar{\gamma}_1}\right)x} x^v dx. \tag{56}$$

The internal integration in I_1 is given by [36, eq. (3.351.3)]

$$\Gamma(1+v)\left(zs+(l/\bar{\gamma}_1)\right)^{-1-v}. \tag{57}$$

Thus, with the help of (56) and (57), I_2 can be calculated as

$$\begin{aligned} I_2 = a_1 e^{\frac{l}{\bar{\gamma}_1}} \sum_{k=0}^{m-1} \frac{(1-m)_k (-a_2)^k}{l^{k+1}(1)_k} \sum_{n=0}^{k} \frac{l^n}{\bar{\gamma}_1^n n!} \sum_{v=0}^{n} \binom{n}{v} \\ \times (-1)^{n-v} \Gamma(1+v) \int_0^{\infty} e^{-s} \left(zs+(l/\bar{\gamma}_1)\right)^{-1-v} ds. \end{aligned} \tag{58}$$

By denoting $\left(zs+(l/\bar{\gamma}_1)\right)^{-1-v}$ as Meijer-G function [51, eq. (01.02.26.0007.01)], and with the help of [36, eq. (7.813.1)], the internal integration in I_2 can be given by

$$\frac{(l/\bar{\gamma}_1)^{-1-v}}{\Gamma(1+v)} \int_0^{\infty} e^{-s} \mathrm{G}_{1,1}^{1,1}\left[\frac{\bar{\gamma}_1}{l} zs \,\middle|\, \begin{matrix} -v \\ 0 \end{matrix}\right] ds = \frac{(l/\bar{\gamma}_1)^{-1-v}}{\Gamma(1+v)} \mathrm{G}_{2,1}^{1,2}\left[\frac{\bar{\gamma}_1}{l} z \,\middle|\, \begin{matrix} 0, -v \\ 0 \end{matrix}\right]. \tag{59}$$

Additionally, by using (52), (58), (59) and $f_Z(z) = C f_{\gamma_2}(Cz)$, $R_{\gamma'}$ can be expressed as

$$\begin{aligned} R_{\gamma'} = \frac{B}{2\ln 2} a_1 e^{\frac{l}{\bar{\gamma}_1}} C \frac{e^{-Z_D^2/(2b_D)}}{2b_D\bar{\gamma}_2} \sum_{k=0}^{m-1} \frac{(1-m)_k (-a_2)^k}{l^{k+1}(1)_k} \\ \times \sum_{n=0}^{k} \frac{l^n}{\bar{\gamma}_1^n n!} \sum_{v=0}^{n} \binom{n}{v} (-1)^{n-v} \left(\frac{l}{\bar{\gamma}_1}\right)^{-1-v} \\ \times \underbrace{\int_0^{\infty} z e^{-\frac{Cz}{2b_D\bar{\gamma}_2}} \mathrm{G}_{2,1}^{1,2}\left[\frac{\bar{\gamma}_1}{l} z \,\middle|\, \begin{matrix} 0, -v \\ 0 \end{matrix}\right] I_0\left(\frac{Z_D}{b_D}\sqrt{\frac{Cz}{\bar{\gamma}_2}}\right) dz}_{I_3}. \end{aligned} \tag{60}$$

By using [51, eq. (03.02.26.0008.01)], the *zero*th-order modified Bessel function of the first kind can be expressed through Meijer-G function as

$$I_0\left(\sqrt{z}\right) = \mathrm{G}_{0,2}^{1,0}\left[-\frac{z}{4} \,\middle|\, \begin{matrix} \\ 0, 0 \end{matrix}\right]. \tag{61}$$

Then with the help of integral formula for multiple Meijer-G functions [51, eq. (07.34.21.0081.01)],

I_3 can be given by

$$\begin{aligned} I_3 &= \int_0^\infty z e^{-\frac{Cz}{2b_D\bar{\gamma}_2}} \mathrm{G}_{2,1}^{1,2}\left[\frac{\bar{\gamma}_1}{l}z \,\middle|\, \begin{matrix} 0,-v \\ 0 \end{matrix}\right] \mathrm{G}_{0,2}^{1,0}\left[-\left(\frac{Z_D}{b_D}\right)^2 \frac{Cz}{4\bar{\gamma}_2} \,\middle|\, 0,0\right] dz \\ &= \left(\frac{2b_D\bar{\gamma}_2}{C}\right)^2 \mathrm{G}_{1,0;2,1;0,2}^{0,0;1,2;1,0}\left[\begin{matrix} 2 \\ \end{matrix} \,\middle|\, \begin{matrix} 0,-v \\ 0 \end{matrix} \,\middle|\, 0,0 \,\middle|\, \frac{\bar{\gamma}_1}{l}, -\left(\frac{Z_D}{b_D}\right)^2 \frac{C}{4\bar{\gamma}_2}\right]. \end{aligned} \tag{62}$$

where $G_{p_1,q_1;p_2,q_2;p_3,q_3}^{m_1,n_1;m_2,n_2;m_3,n_3}[\cdot|\cdot|\cdot]$ denotes the bivariate Meijer-G function.

Moreover, R_Z can be calculated as

$$\begin{aligned} R_Z &= \frac{B}{2\ln 2}\int_0^\infty \ln(1+z) f_Z(z)\, dz \\ &= \frac{B}{2\ln 2} C \frac{e^{-Z_D^2/(2b_D)}}{2b_D\bar{\gamma}_2} \underbrace{\int_0^\infty e^{-\frac{Cz}{2b_D\bar{\gamma}_2}} \ln(1+z)\, \mathrm{G}_{0,2}^{1,0}\left[-\left(\frac{Z_D}{b_D}\right)^2 \frac{Cz}{4\bar{\gamma}_2} \,\middle|\, 0,0\right] dz}_{I_4} \end{aligned} \tag{63}$$

Next, we express $\ln(1+z)$ in terms of Meijer-G functions by using [36, eq. (8.4.6.5)]

$$\ln(1+z) = \mathrm{G}_{2,2}^{1,2}\left[z \,\middle|\, \begin{matrix} 1,1 \\ 1,0 \end{matrix}\right], \tag{64}$$

then with a similar manner, I_4 can be calculated as

$$I_4 = \frac{2b_D\bar{\gamma}_2}{C} \mathrm{G}_{0,1;2,2;0,2}^{1,0;1,2;1,0}\left[\begin{matrix} 1 \\ \end{matrix} \,\middle|\, \begin{matrix} 1,1 \\ 1,0 \end{matrix} \,\middle|\, 0,0 \,\middle|\, \frac{2b_D\bar{\gamma}_2}{C}, -\frac{2b_3 b_D\bar{\gamma}_2}{4C}\right]. \tag{65}$$

Finally, by substituting (60), (62), (63), (65) and (46) into (19), the closed-form energy efficiency expression for the considered system can be obtained as

$$\begin{aligned} \eta \;=& \frac{B}{2(\mu P_R + P_{const})\ln 2}\left(a_1 e^{\frac{l}{\bar{\gamma}_1}} \frac{2b_D\bar{\gamma}_2 e^{-Z_D^2/(2b_D)}}{C} \sum_{k=0}^{m-1} \frac{(1-m)_k (-a_2)^k}{l^{k+1}(1)_k} \sum_{n=0}^{k} \frac{l^n}{\bar{\gamma}_1^n n!}\right. \\ &\times \sum_{v=0}^{n} \binom{n}{v} (-1)^{n-v} \left(\frac{l}{\bar{\gamma}_1}\right)^{-1-v} \mathrm{G}_{1,0;2,1;0,2}^{0,0;1,2;1,0}\left[\begin{matrix} 2 \\ \end{matrix} \,\middle|\, \begin{matrix} 0,-v \\ 0 \end{matrix} \,\middle|\, 0,0 \,\middle|\, \frac{\bar{\gamma}_1}{l}, -\left(\frac{Z_D}{b_D}\right)^2 \frac{C}{4\bar{\gamma}_2}\right] \\ &\left. - e^{-Z_D^2/(2b_D)} \mathrm{G}_{0,1;2,2;0,2}^{1,0;1,2;1,0}\left[\begin{matrix} 1 \\ \end{matrix} \,\middle|\, \begin{matrix} 1,1 \\ 1,0 \end{matrix} \,\middle|\, 0,0 \,\middle|\, \frac{2b_D\bar{\gamma}_2}{C}, -\frac{2b_3 b_D\bar{\gamma}_2}{4C}\right]\right). \end{aligned} \tag{66}$$

Remark 1: Note that the final analytical EE expression contains the bivariate Meijer-G function,

which can be efficiently calculated by the general software tools. For example, an efficient Mathematica implementation for evaluating the bivariate Meijer-G functions fast and accurately was presented in [52]. Therefore, the derived formula provides an effective method to evaluate the EE of the considered SATN.

V. Numerical Results

This section provides computer simulations to confirm the effectiveness and superiority of our proposed BF schemes as well as the validity of the analytical results. The system works at the S band, and we assume that the S-R link undergoes infrequent light shadowing (ILS) with $(m, b, \Omega) = (20, 0.158, 1.29)$ [39], and the Rician factor of R-D link is $K = 10$ [42]. In all plots, the angular spread of AoA equals that of AoD, namely, $\Delta_R = \Delta_D = \Delta$. The noise power at R and D are given by $\sigma_R^2 = \sigma_D^2 = \kappa_B T B$, with $\kappa_B = 1.38 \times 10^{-23}$J/K being Boltzmann constant and $T = 300$ K is the noise temperature. The other main simulation parameters are given in Table I. In addition, the results of Monte Carlo simulations are obtained by performing 10^6 channel realizations.

Table I: Main simulation parameters

Parameter	Value
Orbit	GEO
Maximal satellite beam gain	$G_S^{\max} = 49.5$ dB
Satellite transmit power	$P_S = 20$ dBW
Maximal receive gain at D	$G_D^{\max} = 3$ dB
Array inter-element spacing	$d_e = \lambda/2$
Bandwidth	$B = 5$ MHz
Path loss factor of R-D link	$\alpha_D = 2.5$
Angle-of-arrival	$\theta_r = 40^\circ$
Angle-of-departure	$\theta_t = 30^\circ$
Height of UAV	$H_R = 500$ m
Circuit power of each antenna	$P_c = 10$ dBmW
Static power at UAV	$P_0 = 30$ dBmW
Power amplifier inefficiency coefficient	$\mu = 2.6$

Since the calculation of the ergodic capacity R_{EC} is the key point to evaluate the EE of the considered system, we firstly validate the analytical expression given in (66). By assuming that N =32 or 64 and $\Delta = 5^\circ$, the curves of EC against the transmit power P_R at UAV are shown in Fig. 2, where the approximate EC calculated with (21) through Jensen's inequality, the exact EC computed with (66), and the EC via Monte Carlo simulations are denoted as 'Approximate', 'Analytical' and 'Monte Carlo', respectively. As seen, the analytical results computed with (66)

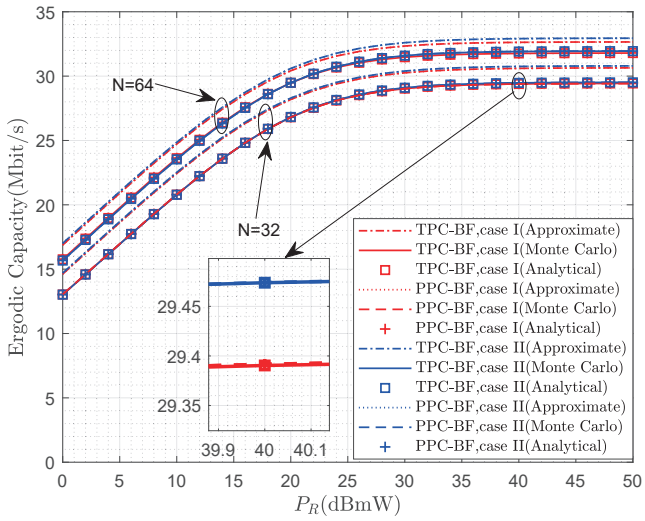

Fig. 2. EC versus P_R for the SATN with $\Delta = 5°$

match well with Monte Carlo simulations, and both of them are a bit lower than the approximate results through Jensen's inequality, implying that our derived theoretical formula can accurately evaluate the EC of the system. However, considering the fact that the curve shapes of approximate EC are similar to those of exact EC, and the performance gap is less than 4%, we can conclude that Jensen's inequality is an effective method to simplify EEM problem in (20). Meanwhile, it can be observed that the performance of PPC-BF scheme is a bit worse than that of the TPC-BF scheme. This is because the former scheme approximates the CCM with the first term of Taylor's expression. But the performance gap can be neglected. Furthermore, since the scattering power of case II is more concentrated than that of case I, the EC of the SATN in case II is slightly higher than that in case I, meaning that our schemes are applicable for the high correlated channels, which cope with UAV application.

Secondly, by assuming that the UAV is deployed with 64-element ULA and the angular spread is 5°, Figs. 3 and 4 depict the maximum EE of the considered system versus the maximum transmit power $P_R^{\max}$ in case I and case II, respectively. Here, the results of the spectral efficiency maximization (SEM) scheme in [6] and EEM scheme in [47], both of which employing perfect CSI are also provided for comparison purposes. As illustrated, when $P_R^{\max} \leq 18$ dBmW, the EEs of all schemes are enhanced with the increase of maximum transmit power. This is because full transmit power $P_R^{\max}$ is exploited in this occasion. However, in the scenario where $P_R^{\max} \geq 18$ dBmW, since the SEM scheme in [6] still employs full transmit power, while our

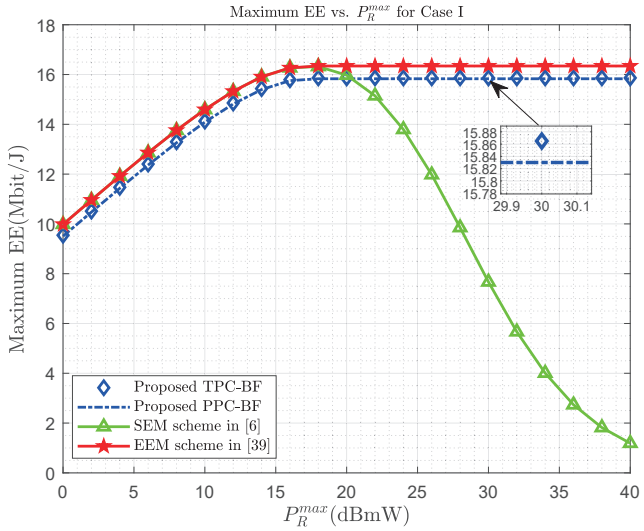

Fig. 3. Maximum EE versus $P_R^{\max}$ with different schemes in Case I

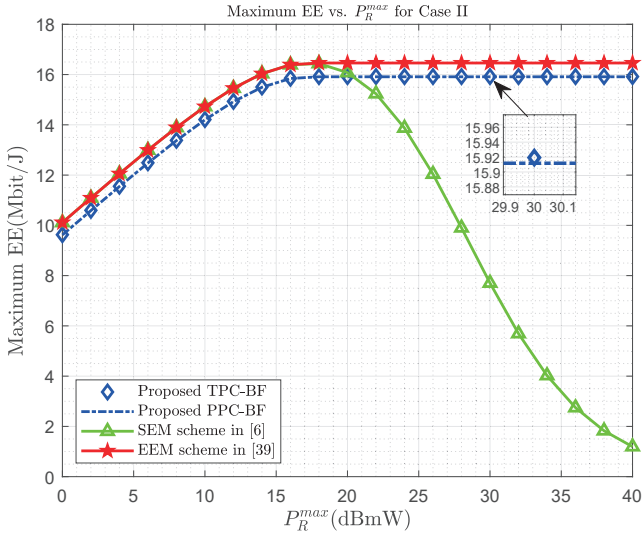

Fig. 4. Maximum EE versus $P_R^{\max}$ with different schemes in Case II

proposed schemes and the EEM scheme in [47] cease transmit more power based on the power allocation procedure to avoid sacrificing the achieved EE, whereas that of the former scheme is degraded significantly as $P_R^{\max}$ increases. Additionally, the TPC-BF scheme outperforms the PPC-BF scheme with a negligible superiority. This is because that the PPC-BF scheme employs an approximation to obtain the BF vectors due to the per-antenna power constraint. Furthermore, it is worth mentioning that although there exists a small EE gap between our schemes and the EEM scheme in [47], which employs perfect CSI and convex optimization packages to obtain

the optimal solution, the performance gap is, however, neglectable, resulting in the conclusion that our proposed schemes can achieve satisfied performance with low complexity.

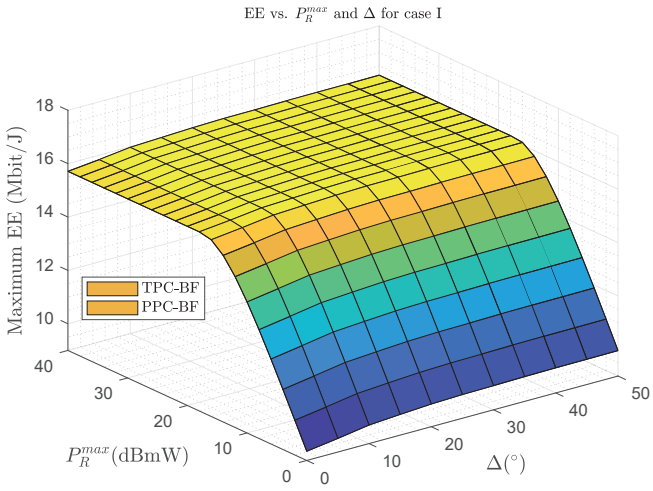

Fig. 5. Maximum EE versus $P_R^{\max}$ and Δ for Case I

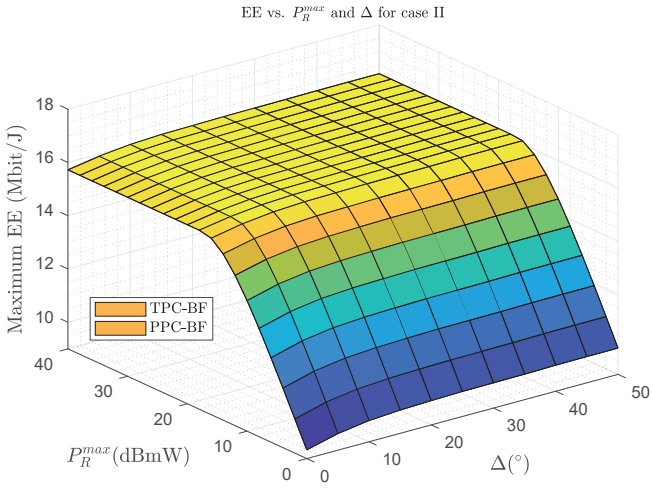

Fig. 6. Maximum EE versus $P_R^{\max}$ and Δ for Case II

Finally, to verify the impact of angular spread Δ on the proposed schemes, we suppose that a 64-element array is employed at UAV, and show the maximum EEs for the considered system in case I and case II, respectively. Just as we expected, with the increase of $P_R^{\max}$, the maximum EE of each proposed scheme is enhanced at first, and then reach and keep a certain level. In addition, it can be found that when the angular spread Δ varies from 0° to 50°, the EE performance of our schemes changes slightly, meaning that the proposed methods are robust to the angular spread.

Since the angular spread is often less than 15° in high correlated channels due to the lack of scattering, our BF schemes are valuable for the UAV application.

VI. Conclusion

In this paper, we have studied the energy efficient transmission for a SATN, with a multi-antenna UAV being used as an aerial relay. We have first established an EEM problem for the SATN under two different power constraints. Then we have jointly exploited ASP technique together with the Dinkelbach's method, and proposed two BF schemes with low implementation complexity, whose results are given in analytical expressions. It has been shown that the performance gap between the proposed schemes and the perfect CSI-based optimal solution are neglectable. Furthermore, the EE for the considered SATN has been derived in new analytical expressions, and numerical results have validated the theoretical formulas.

Appendix A
Proof of Lemma 1

We first consider (23), according to (4), the CCM of $\mathbf{g}_R$ can be calculated as

$$\begin{aligned}\mathbf{\Phi}_R &= \mathbb{E}_{\mathbf{g}_R}\left[\left(\bar{\mathbf{g}}_R+\tilde{\mathbf{\Phi}}_R^{1/2}\tilde{\mathbf{g}}_R\right)\left(\bar{\mathbf{g}}_R+\tilde{\mathbf{\Phi}}_R^{1/2}\tilde{\mathbf{g}}_R\right)^H\right] \\ &= \mathbb{E}_{\mathbf{g}_R}\left[\bar{\mathbf{g}}_R\bar{\mathbf{g}}_R^H\right]+\mathbb{E}_{\mathbf{g}_R}\left[\bar{\mathbf{g}}_R\tilde{\mathbf{g}}_R^H\right]\tilde{\mathbf{\Phi}}_R^{H/2}+\tilde{\mathbf{\Phi}}_R^{1/2}\mathbb{E}_{\mathbf{g}_R}\left[\tilde{\mathbf{g}}_R\bar{\mathbf{g}}_R^H\right]+\tilde{\mathbf{\Phi}}_R^{1/2}\mathbb{E}_{\mathbf{g}_R}\left[\tilde{\mathbf{g}}_R\tilde{\mathbf{g}}_R^H\right]\tilde{\mathbf{\Phi}}_R^{H/2}.\end{aligned} \tag{67}$$

Following (5), the first term of (67) is given by

$$\mathbb{E}\left[\bar{\mathbf{g}}_R\bar{\mathbf{g}}_R^H\right]=\mathbb{E}\left[Z_R^2\right]\mathbf{a}\left(\theta_r\right)\mathbf{a}^H\left(\theta_r\right)=\Omega\mathbf{a}\left(\theta_r\right)\mathbf{a}^H\left(\theta_r\right). \tag{68}$$

By using $\tilde{\mathbf{g}}_R\sim(\mathbf{0},2b\mathbf{I}_N)$, and considering that $\bar{\mathbf{g}}_R$ and $\tilde{\mathbf{g}}_R$ are independent with each other, both of the second and third terms in (67) equal zero vector, while the last term of (67) can be obtained as

$$\tilde{\mathbf{\Phi}}_R^{1/2}\mathbb{E}_{\mathbf{g}_R}\left[\tilde{\mathbf{g}}_R\tilde{\mathbf{g}}_R^H\right]\tilde{\mathbf{\Phi}}_R^{H/2}=2b\tilde{\mathbf{\Phi}}_R^{1/2}\mathbf{I}_N\tilde{\mathbf{\Phi}}_R^{H/2}=2b\tilde{\mathbf{\Phi}}_R. \tag{69}$$

As a result, (67) can be simplified as

$$\mathbf{\Phi}_R=\Omega\mathbf{a}\left(\theta_r\right)\mathbf{a}^H\left(\theta_r\right)+2b\tilde{\mathbf{\Phi}}_R. \tag{70}$$

As for $\tilde{\mathbf{\Phi}}_R$, based on the widely used scattering cluster model [53], it can be calculated as

$$\tilde{\mathbf{\Phi}}_R = \int_{-\infty}^{\infty} \mathbf{a}\left(\tilde{\theta}_r\right) \mathbf{a}^H\left(\tilde{\theta}_r\right) f_{\tilde{\theta}_r}\left(\tilde{\theta}_r\right) d\tilde{\theta}_r, \tag{71}$$

where $f_{\tilde{\theta}_r}(\theta)$ denotes the scattering power distribution, which is often assumed to satisfy uniform distribution termed as case I and Gaussian distribution termed as case II, respectively. The mathematical formulas are given by

$$f_{\tilde{\theta}_r}\left(\tilde{\theta}_r\right) = \begin{cases} \frac{1}{\Delta_r}, \theta_r - \frac{\Delta_r}{2} \le \tilde{\theta}_r \le \theta_r + \frac{\Delta_r}{2}, \text{ caseI} \\ \frac{2\sqrt{2}}{\sqrt{\pi}\Delta_r} e^{-\frac{8\left(\tilde{\theta}_r - \theta_r\right)^2}{\Delta_r^2}}, \text{ caseII} \end{cases}, \tag{72}$$

where Δ_r is the angular spread associated with AoA θ_r.

As for case I, by using (71) and (72) and letting $\tilde{\theta}_r = \theta_r + \theta$, the mn-th element of $\tilde{\mathbf{\Phi}}_R$ can be obtained as

$$\left[\tilde{\mathbf{\Phi}}_R\right]_{m,n} = \frac{1}{\Delta_r} \int_{-\Delta_r/2}^{\Delta_r/2} e^{j(m-n)\kappa d_e \sin(\theta_r + \theta)} d\theta. \tag{73}$$

With the help of the approximate formula $\sin(\theta_r + \theta) \approx \sin\theta_r + \theta\cos\theta_r$, after some algebraic manipulations, the closed-form expression of (73) is given by

$$\left[\tilde{\mathbf{\Phi}}_R\right]_{m,n} \approx e^{j(m-n)\kappa d_e \sin\theta_r} \frac{\sin\left((m-n)\kappa d_e \frac{\Delta_r}{2}\cos\theta_r\right)}{(m-n)\kappa d_e \frac{\Delta_r}{2}\cos\theta_r}. \tag{74}$$

Concerning case II, by substituting (72) into (71) and using approximation for $\sin(\theta_r + \theta)$, $\left[\tilde{\mathbf{\Phi}}_R\right]_{m,n}$ can be obtained as

$$\left[\tilde{\mathbf{\Phi}}_R\right]_{m,n} \approx e^{j(m-n)\kappa d_e \sin\theta_r} \mathrm{e}^{-\frac{\Delta_r^2}{32}\left((m-n)\kappa d_e \cos\theta_r\right)^2}. \tag{75}$$

By using (74) and (75) into (70), $[\mathbf{\Phi}_R]_{m,n}$ is given by (23).

Next, we focus on (24). Based on (10), $\mathbf{\Phi}_D$ can be written as

$$\begin{aligned} \mathbf{\Phi}_D = & \frac{K}{K+1}\mathbb{E}_{\mathbf{g}_D}\left[\bar{\mathbf{g}}_D \bar{\mathbf{g}}_D^H\right] + \frac{\sqrt{K}}{K+1}\mathbb{E}_{\mathbf{g}_D}\left[\bar{\mathbf{g}}_D \tilde{\mathbf{g}}_D^H\right] \tilde{\mathbf{\Phi}}_D^{H/2} \\ & + \frac{\sqrt{K}}{K+1}\tilde{\mathbf{g}}_D^{1/2}\mathbb{E}_{\mathbf{g}_D}\left[\tilde{\mathbf{\Phi}}_D \bar{\mathbf{g}}_D^H\right] + \frac{1}{K+1}\tilde{\mathbf{\Phi}}_D^{1/2}\mathbb{E}_{\mathbf{g}_D}\left[\tilde{\mathbf{g}}_D \tilde{\mathbf{g}}_D^H\right] \tilde{\mathbf{\Phi}}_D^{H/2}. \end{aligned} \tag{76}$$

Similarly, the second and third terms in (76) equal zero vector, while the first and last terms in (76) are, respectively, given by $\frac{K}{K+1}\mathbf{a}(\theta_t)\mathbf{a}^H(\theta_t)$ and $\frac{1}{K+1}\tilde{\mathbf{\Phi}}_D$. Therefore, (76) can be simplified

as

$$\mathbf{\Phi}_D = \frac{K}{K+1}\mathbf{a}(\theta_t)\,\mathbf{a}^H(\theta_t) + \frac{1}{K+1}\tilde{\mathbf{\Phi}}_D. \tag{77}$$

With a similar manner in the derivation of $[\mathbf{\Phi}_R]_{m,n}$, by using the scattering cluster model and the approximation $\sin(\theta_t+\theta) \approx \sin\theta_t + \theta\cos\theta_t$, after some algebraic manipulations, the mn-th element of $\mathbf{\Phi}_D$ can be expressed as (24).

Appendix B
Proof of Lemma 2

As for the CDF of $\gamma_1 = \bar{\gamma}_1\left|\mathbf{w}_r^H\mathbf{g}_R\right|^2$ with $\bar{\gamma}_1 = P_S/\rho_R^2$, by denoting $\tilde{\mathbf{g}}_R = \left[g_{R,1},\ldots,g_{R,N}\right]$ and $\mathbf{w}_r^H\tilde{\mathbf{\Phi}}_R^{1/2} = \mathbf{V} = [V_1,\ldots,V_N] = \left[|V_1|\,e^{j\xi_1},\ldots,|V_N|\,e^{j\xi_N}\right]$, and using (4), after some trivial computation, we have

$$\mathbf{w}_r^H\mathbf{g}_R = Z_R\mathbf{w}_r^H\mathbf{a}(\theta_r) + \mathbf{w}_r^H\tilde{\mathbf{\Phi}}_R^{1/2}\tilde{\mathbf{g}}_R = Z_R\mathbf{w}_r^H\mathbf{a}(\theta_r) + \sum_{n=1}^{N}|V_n|\,g_{R,n}e^{j\xi_n}. \tag{78}$$

In deriving (78), we have utilized the fact that since BF weight vector $\mathbf{w}_r$ is obtained based on the AI-CSI, thus $\mathbf{w}_r^H\tilde{\mathbf{\Phi}}_R^{1/2} \in \mathbb{C}^{1\times N}$ is a constant vector. Furthermore, as we mentioned previously, $g_{R,n} \sim \mathbb{CN}(0,2b)$ is a complex Gaussian RV, thus $g_{R,n}e^{j\xi_n} = X_n + jY_n$ is also a complex Gaussian RV with $X_n, Y_n \sim \mathbb{N}(0,b)$, resulting in $\sum_{n=1}^{N}|V_n|\,X_n$, $\sum_{n=1}^{N}|V_n|\,Y_n \sim \mathbb{N}\left(0, b\|\mathbf{V}\|^2\right)$. Consequently, if we rewrite (78) as

$$\mathbf{w}_r^H\mathbf{g}_R = Z_R\mathbf{w}_r^H\mathbf{a}(\theta_r) + \left(\sum_{n=1}^{N}|V_n|\,X_n + j\sum_{n=1}^{N}|V_n|\,Y_n\right), \tag{79}$$

we find that the second term of (79) is a complex Gaussian RV with average power $2b\|\mathbf{V}\|^2 = 2b\left\|\mathbf{w}_r^H\tilde{\mathbf{\Phi}}_R^{1/2}\right\|^2$, and the PDF of $h_1 = \left|\mathbf{w}_r^H\mathbf{g}_R\right|$ can be calculated as [39]

$$f_{h_1}(x) = \mathbb{E}_{Z_R'}\left[\frac{x}{b_R}\exp\left(-\frac{x^2+{Z_R'}^2}{2b_R}\right)I_0\left(\frac{Z_R'x}{b_R}\right)\right], \tag{80}$$

where $Z_R' = Z_R\mathbf{w}_r^H\mathbf{a}(\theta_r)$ is a Nakagami-m RV with average power $\left|\mathbf{w}_r^H\mathbf{a}(\theta_r)\right|^2\Omega$ and severity parameter m, and $b_R = b\left\|\mathbf{w}_r^H\tilde{\mathbf{\Phi}}_R^{1/2}\right\|^2$. By calculating the expectation of (80) with respect to the Nakagami distribution of Z_R', and after some algebraic manipulations, (80) can be rewritten as

$$f_{h_1}(x) = \left(\frac{2b_Rm}{2b_Rm+\left|\mathbf{w}_r^H\mathbf{a}(\theta_r)\right|^2\Omega}\right)^m\frac{x}{b_R}\exp\left(-\frac{x^2}{2b_R}\right){}_1F_1\left(m,1,\frac{\left|\mathbf{w}_r^H\mathbf{a}(\theta_r)\right|^2\Omega x^2}{2b_R\left(2b_Rm+\left|\mathbf{w}_r^H\mathbf{a}(\theta_r)\right|^2\Omega\right)}\right). \tag{81}$$

Then, the PDF of $\gamma_1 = \bar{\gamma}_1 \left|\mathbf{w}_r^H \mathbf{g}_R\right|^2 = \bar{\gamma}_1 h_1^2$ can be obtained as

$$f_{\gamma_1}(x) = \frac{1}{2\sqrt{\bar{\gamma}_1 x}} f_{r_1}\left(\sqrt{x/\bar{\gamma}_1}\right) = \frac{a_1}{\bar{\gamma}_1} \exp\left(-\frac{x}{2b_R\bar{\gamma}_1}\right) {}_1F_1\left(m, 1, \frac{a_2 x}{\bar{\gamma}_1}\right), \tag{82}$$

where a_1, a_2 are given in (53) and (54), respectively. In this paper, we make a reasonable assumption of $m \in \mathbb{N}^+$ [4], [50]. With the help of [54], then the PDF of γ_1 in the case of $m \in \mathbb{N}^+$ can be expressed as finite series expansion, namely,

$$f_{\gamma_1}(x) = a_1 e^{-(1/(2b_R)-a_2)\frac{x}{\bar{\gamma}_1}} \sum_{k=0}^{m-1} \frac{(1-m)_k (-a_2)^k}{\bar{\gamma}_1^{k+1} (1)_k k!} x^k. \tag{83}$$

By using (83) and resorting to [36, eq.(3.351.1)], the CDF of γ_1 can be obtained as (51). Furthermore, C in (17) can be calculated as

$$C = 1 + \int_0^\infty x f_{\gamma_1}(x)\, dx. \tag{84}$$

By substituting (83) into (84), and with the help of [36, eq. (3.351.3)], the coefficient C can be expressed as (55).

Next, we focus on the PDF of $\gamma_2 = \bar{\gamma}_2 \left|\mathbf{w}_t^H \mathbf{g}_D\right|^2$ with $\bar{\gamma}_2 = P_R / \rho_D^2$. With the help of (10), $\mathbf{w}_t^H \mathbf{g}_D$ can be denoted as

$$\mathbf{w}_t^H \mathbf{g}_D = \sqrt{\frac{K}{K+1}} \mathbf{w}_t^H \mathbf{a}(\theta_t) + \sqrt{\frac{1}{K+1}} \mathbf{w}_t^H \tilde{\mathbf{\Phi}}_D^{1/2} \tilde{\mathbf{g}}_D. \tag{85}$$

Similar to the derivation process of γ_1, $\mathbf{w}_t^H \mathbf{g}_D$ can be reformulated as the sum of a constant $Z_D = \sqrt{K/(K+1)} \left|\mathbf{w}_t^H \mathbf{a}(\theta_t)\right|$ and a complex Gaussian RV with the average power $2b_D = \left\|\mathbf{w}_t^H \tilde{\mathbf{\Phi}}_D^{1/2}\right\|^2 / (K+1)$, where the closed-form expression for $\tilde{\mathbf{\Phi}}_D$ is given as the last term of $\mathbf{\Phi}_D$ in (24). According to the statistical property of complex Gaussian RV, the PDF of $h_2 = \left|\mathbf{w}_t^H \mathbf{g}_D\right|$ can be expressed as

$$f_{h_2}(x) = \frac{x}{b_D} \exp\left(-\frac{x^2 + Z_D^2}{2b_D}\right) I_0\left(\frac{Z_D x}{b_D}\right), \tag{86}$$

where $I_n(\cdot)$ is the nth-order modified Bessel function of the first kind. Finally, by using $f_{\gamma_2}(x) = \frac{1}{2\sqrt{\bar{\gamma}_2 x}} f_{h_2}\left(\sqrt{x/\bar{\gamma}_2}\right)$, the PDF of $\gamma_2 = \bar{\gamma}_2 h_2^2$ can be obtained as (52).

REFERENCES

[1] M. Jia, X. Gu, Q. Guo, W. Xiang, and N. Zhang, "Broadband hybrid satellite-terrestrial communication systems based on cognitive radio toward 5G," *IEEE Wireless Commun.*, vol. 23, no. 6, pp. 96–106, 2016.

[2] K. An, M. Lin, J. Ouyang, and W.-P. Zhu, "Secure transmission in cognitive satellite terrestrial networks," *IEEE J. Sel. Areas Commun.*, vol. 34, no. 11, pp. 3025 – 3037, 2016.

[3] G. Giambene, S. Kota, and P. Pillai, "Satellite-5G integration: A network perspective," *IEEE Netw.*, vol. 32, no. 5, pp. 25–31, 2018.

[4] Y. Ruan, Y. Li, C. X. Wang, and R. Zhang, "Energy efficient adaptive transmissions in integrated satellite-terrestrial networks with SER constraints," *IEEE Trans. Wireless Commun.*, vol. 17, no. 1, pp. 210–222, 2018.

[5] T. ETSI, "102 585 (2008-04): Digital Video Broadcasting (DVB)," *System Specifications for Satellite Services to Handheld Devices below 3GHz*.

[6] M. K. Arti and M. R. Bhatnagar, "Beamforming and combining in hybrid satellite-terrestrial cooperative systems," *IEEE Commun. Lett.*, vol. 18, no. 3, pp. 483–486, 2014.

[7] K. An, M. Lin, T. Liang, J.-B. Wang, J. Wang, Y. Huang, and A. L. Swindlehurst, "Performance analysis of multi-antenna hybrid satellite-terrestrial relay networks in the presence of interference," *IEEE Trans. Commun.*, vol. 63, no. 11, pp. 4390–4404, 2015.

[8] V. Bankey, P. K. Upadhyay, D. B. D. Costa, P. S. Bithas, A. G. Kanatas, and U. S. Dias, "Performance analysis of multi-antenna multiuser hybrid satellite-terrestrial relay systems for mobile services delivery," *IEEE Access*, vol. 6, pp. 24 729–24 745, 2018.

[9] K. An, J. Ouyang, M. Lin, and T. Liang, "Outage analysis of multi-antenna cognitive hybrid satellite-terrestrial relay networks with beamforming," *IEEE Commun. Lett.*, vol. 19, no. 7, pp. 1157–1160, 2015.

[10] Q. Huang, M. Lin, W.-P. Zhu, S. Chatzinotas, and M.-S. Alouini, "Performance analysis of integrated satellite-terrestrial multiantenna relay networks with multiuser scheduling," *IEEE Trans. Aerosp. Electron. Syst.*, pp. 1–1, 2019.

[11] H. Zhu and J. Wang, "Chunk-based resource allocation in OFDMA systems-part I: chunk allocation," *IEEE Trans. Commun.*, vol. 57, no. 9, pp. 2734–2744, 2009.

[12] ——, "Chunk-based resource allocation in OFDMA systems-part II: Joint chunk, power and bit allocation," *IEEE Trans. Commun.*, vol. 60, no. 2, pp. 499–509, 2012.

[13] I. Bor-Yaliniz and H. Yanikomeroglu, "The new frontier in RAN heterogeneity: Multi-tier drone-cells," *IEEE Commun. Mag.*, vol. 54, no. 11, pp. 48–55, 2016.

[14] A. A. Khuwaja, Y. Chen, N. Zhao, M.-S. Alouini, and P. Dobbins, "A survey of channel modeling for UAV communications," *IEEE Commun. Surveys Tuts.*, vol. 20, no. 4, pp. 2804–2821, 2018.

[15] Y. Zeng, J. Lyu, and R. Zhang, "Cellular-connected UAV: Potential, challenges and promising technologies," *IEEE Wireless Commun.*, pp. 1–8, 2018.

[16] N. Zhao, W. Lu, M. Sheng, Y. Chen, J. Tang, F. R. Yu, and K. Wong, "UAV-assisted emergency networks in disasters," *IEEE Wireless Commun.*, vol. 26, no. 1, pp. 45–51, 2019.

[17] P. Zhan, K. Yu, and A. L. Swindlehurst, "Wireless relay communications with unmanned aerial vehicles: Performance and optimization," *IEEE Trans. Aerosp. Electron. Syst.*, vol. 47, no. 3, pp. 2068–2085, 2011.

[18] J. Zhao, F. Gao, Q. Wu, S. Jin, Y. Wu, and W. Jia, "Beam tracking for UAV mounted satcom on-the-move

with massive antenna array," *IEEE J. Sel. Areas Commun.*, vol. 36, no. 2, pp. 363–375, 2018.

[19] M. Lin, J. Ouyang, and W.-P. Zhu, "Joint beamforming and power control for device-to-device communications underlaying cellular networks," *IEEE J. Sel. Areas Commun.*, vol. 34, no. 1, pp. 138–150, 2016.

[20] Z. Lin, M. Lin, J.-B. Wang, Y. Huang, and W.-P. Zhu, "Robust secure beamforming for 5G cellular networks coexisting with satellite networks," *IEEE J. Sel. Areas Commun.*, pp. 932–945, 2018.

[21] Z. Xiao, P. Xia, and X. Xia, "Enabling UAV cellular with millimeter-wave communication: potentials and approaches," *IEEE Commun. Mag.*, vol. 54, no. 5, pp. 66–73, 2016.

[22] L. Sboui, H. Ghazzai, Z. Rezki, and M.-S. Alouini, "Achievable rates of UAV-relayed cooperative cognitive radio mimo systems," *IEEE Access*, vol. 5, pp. 5190–5204, 2017.

[23] Q. Song, S. Jin, and F. Zheng, "Joint power allocation and beamforming for UAV-enabled relaying systems with channel estimation errors," in *2018 IEEE 87th Veh. Technol. Conf. (VTC Spring)*, Conf. Proc., pp. 1–5.

[24] Y. Zeng and R. Zhang, "Energy-efficient UAV communication with trajectory optimization," *IEEE Trans. Wireless Commun.*, vol. 16, no. 6, pp. 3747–3760, 2017.

[25] M. Mozaffari, W. Saad, M. Bennis, and M. Debbah, "Optimal transport theory for power-efficient deployment of unmanned aerial vehicles," in *2016 IEEE Int. Conf. Commun. (ICC)*, Conf. Proc., pp. 1–6.

[26] L. Sboui, H. Ghazzai, Z. Rezki, and M.-S. Alouini, "Energy-efficient power allocation for UAV cognitive radio systems," in *2017 IEEE 86th Veh. Technol. Conf. (VTC Fall)*, Conf. Proc., pp. 1–5.

[27] Q. Song and F. Zheng, "Energy efficient multi-antenna UAV-enabled mobile relay," *China Commun.*, vol. 15, no. 5, pp. 41–50, 2018.

[28] P. K. Sharma, D. Deepthi, and D. I. Kim, "Outage probability of 3D mobile UAV relaying for hybrid satellite-terrestrial networks," *IEEE Commun. Lett.*, pp. 1–1, 2019.

[29] "ABSOLUTE (Aerial Base Stations with Opportunistic Links for Unexpected and Temporary Events). EU FP7 Integrated Project," *Available at http://www.absolute-project.eu/.*

[30] R. Sun, Y. Wang, and Y. Xu, "Downlink energy efficiency power allocation for OFDM-based aerial system with limited satellite backhaul," in *2015 7th Int. Conf. Advances in Satellite and Space Commun. (SPACOMM)*, Conf. Proc..

[31] Y. Xu, Y. Wang, R. Sun, and Y. Zhang, "Joint relay selection and power allocation for maximum energy efficiency in hybrid satellite-aerial-terrestrial systems," in *2016 IEEE 27th Annual Int. Symposium on Personal, Indoor, and Mobile Radio Commun. (PIMRC)*, Conf. Proc., pp. 1–6.

[32] W. Feng, J. Wang, Y. Chen, X. Wang, N. Ge, and J. Lu, "UAV-aided MIMO communications for 5G internet of things," *IEEE Internet Things J.*, vol. 6, no. 2, pp. 1731–1740, 2019.

[33] X. Wang, W. Feng, Y. Chen, and N. Ge, "UAV swarm-enabled aerial CoMP: A physical layer security perspective," *IEEE Access*, vol. 7, pp. 120 901–120 916, 2019.

[34] C. Liu, W. Feng, J. Wang, Y. Chen, and N. Ge, "Aerial small cells using coordinated multiple UAVs: An energy efficiency optimization perspective," *IEEE Access*, vol. 7, pp. 122 838–122 848, 2019.

[35] A. L. Swindlehurst, G. S.-G. B. Jeffs, and J. Li, *Applications of Array Signal Processing: Volume 2,*

Communications and Radar Signal Processing. Academic Press Library in Signal Processing: Elsevier B.V., 2013.

[36] I. S. Gradshteyn and I. M. Ryzhik, *Table of integrals, series, and products*, 8th ed. Academic press, 2014.

[37] K. Storek and A. Knopp, "Fair user grouping for multibeam satellites with MU-MIMO precoding," in *GLOBECOM 2017 - 2017 IEEE Global Commun. Conf.*, Conf. Proc., pp. 1–7.

[38] K. Guo, M. Lin, B. Zhang, W.-P. Zhu, J. Wang, and T. A. Tsiftsis, "On the performance of LMS communication with hardware impairments and interference," *IEEE Trans. Commun.*, vol. 67, no. 2, pp. 1490–1505, 2019.

[39] A. Abdi, W. Lau, M.-S. Alouini, and M. Kaveh, "A new simple model for land mobile satellite channels: first- and second-order statistics," *IEEE Trans.Wireless Commun.*, vol. 2, no. 3, pp. 519–528, 2003.

[40] V. Bankey and P. K. Upadhyay, "Ergodic capacity of multiuser hybrid satellite-terrestrial fixed-gain AF relay networks with CCI and outdated CSI," *IEEE Trans. Veh. Technol.*, vol. 67, no. 5, pp. 4666–4671, 2018.

[41] R. B. Ertel, P. Cardieri, K. W. Sowerby, T. S. Rappaport, and J. H. Reed, "Overview of spatial channel models for antenna array communication systems," *IEEE Pers. Commun.*, vol. 5, no. 1, pp. 10–22, 1998.

[42] F. Jiang and A. L. Swindlehurst, "Optimization of UAV heading for the ground-to-air uplink," *IEEE J. Sel. Areas Commun.*, vol. 30, no. 5, pp. 993–1005, 2012.

[43] L. Sboui, Z. Rezki, and M.-S. Alouini, "Energy-efficient power allocation for MIMO-SVD systems," *IEEE Access*, vol. 5, pp. 9774–9784, 2017.

[44] C. Pan, H. Ren, M. Elkashlan, A. Nallanathan, and L. Hanzo, "Weighted sum-rate maximization for the ultra-dense user-centric TDD C-RAN downlink relying on imperfect CSI," *IEEE Trans. Wireless Commun.*, vol. 18, no. 2, pp. 1182–1198, 2019.

[45] J. Yuan, M. Matthaiou, S. Jin, and F. Gao, "Tightness of Jensen's bounds and applications to MIMO communications," *IEEE Trans. on Commun.*, vol. 65, no. 2, pp. 579–593, 2017.

[46] W. Dinkelbach, "On nonlinear fractional programming," *Manag. Sci.*, vol. 13, no. 7, pp. 492–498, 1967.

[47] J. Ouyang, M. Lin, W.-P. Zhu, T. Hong, and B. Xu, "Distributed-relay beamforming for secrecy energy efficiency with coordinated eavesdroppers," *IEEE Commun. Lett.*, vol. 22, no. 5, pp. 1054–1057, 2018.

[48] P. Chen, J. Ouyang, W.-P. Zhu, and M. Lin, "Energy efficient beamforming for multi-user transmission in cognitive radio networks with secrecy constraints," *IEEE Access*, vol. 6, pp. 74 485–74 493, 2018.

[49] Z. Lin, M. Lin, J.-B. Wang, T. D. Cola, and J. Wang, "Joint beamforming and power allocation for satellite-terrestrial integrated networks with non-orthogonal multiple access," *IEEE J. Sel. Topics Signal Process.*, pp. 1–1, 2019.

[50] N. I. Miridakis, D. D. Vergados, and A. Michalas, "Dual-hop communication over a satellite relay and shadowed Rician channels," *IEEE Trans. Veh. Technol.*, vol. 64, no. 9, pp. 4031–4040, 2015.

[51] I. Wolfram, "Mathematica edition: Version 12.0," 2019.

[52] I. S. Ansari, S. Al-Ahmadi, F. Yilmaz, M.-S. Alouini, and H. Yanikomeroglu, "A new formula for the BER of binary modulations with dual-branch selection over generalized-K composite fading channels," *IEEE Trans. Commun.*, vol. 59, no. 10, pp. 2654–2658, 2011.

[53] B. Friedlander and S. Scherzer, "Beamforming versus transmit diversity in the downlink of a cellular communications system," *IEEE Trans. Veh. Technol.*, vol. 53, no. 4, pp. 1023–1034, 2004.

[54] J. Lopez-Fernandez, J. F. Paris, and E. Martos-Naya, "Bivariate Rician shadowed fading model," *IEEE Trans. Veh. Technol.*, vol. 67, no. 1, pp. 378–384, 2018.